Liu, L.; Puga, AV.; Cored-Bandrés, J.; Concepción Heydorn, P.; Pérez-Dieste, V.; García Gómez, H.; Corma Canós, A. (05-1). Sunlight-assisted hydrogenation of CO2 into ethanol and C2+ hydrocarbons by sodium-promoted Co@C nanocomposites. Applied Catalysis B Environmental. 235:186-196. https://doi.org/10.1016/j.apcatb.2018.04.060

Sunlight-assisted Hydrogenation of CO_2 into ethanol and C2+ Hydrocarbons by Sodium-promoted Co@C Nanocomposites

Lichen Liu,[†] Alberto V. Puga,[†] Jorge Cored,[†] Patricia Concepcion,[†] Virginia Pérez-Dieste,[‡] Hermenegildo García[†]* and Avelino Corma[†]*

† *Instituto de Tecnología Química, Universitat Politècnica de València-Consejo Superior de Investigaciones Científicas (UPV-CSIC), Avenida de los Naranjos s/n, 46022 Valencia, Spain*

‡ *ALBA synchrotron light source, 08290 Cerdanyola del Vallès, Barcelona, Spain*

Corresponding Authors
acorma@itq.upv.es (A.C.)
hgarcia@qim.upv.es (H.G.)

Broader Context

Photoassisted reduction of CO_2 is a sustainable approach for utilization of solar energy and production of solar fuels. So far, the artificial photosynthesis based on CO_2+H_2O usually show very low efficiency due to the thermodynamics and kinetic problems. Considering that low-cost H_2 could be available from electrocatalytic water splitting based on solar cells, reduction of CO_2 with H_2 towards the production of hydrocarbons or oxygenates is an alternative way for more efficient production of solar fuels. Photoassisted hydrogenation of CO_2 has already been reported based on metal or metal oxide catalysts. However, in most of the previous works, the major products are CO and CH_4, with negligible yields of more desired C2+ hydrocarbons. In this work, it will be shown the photoassisted hydrogenation of CO_2 into hydrocarbons (CH_4 together with a high proportion of C2+ hydrocarbons and ethanol) using Na-promoted Co nanoparticles covered by thin carbon layers as catalysts under solar light and near-atmospheric pressure. The reaction rate of this process is in the order of mmol g_{cat}^{-1} h^{-1} and the selectivity to ethanol is 6.5% at 33% CO_2 conversion and 36% selectivity to C2+ hydrocarbons at nearly 100% CO_2 conversion. The reaction mechanism and the role of sunlight irradiation has been investigated by near ambient-pressure X-ray photoelectron (AP-XPS) and *in situ* Raman spectroscopies, providing new insights for understanding photoassited catalytic reactions.

Abstract

The hydrogenation of CO_2 into hydrocarbons promoted by the action of sunlight has been studied on Co nanoparticles covered by thin carbon layers. In particular, nearly 100% selectivity to hydrocarbons is obtained with increased selectivity's towards C2+ hydrocarbons and alcohols (mainly ethanol) when using nanostructured materials comprising metallic cobalt nanoparticles, carbon layers, and sodium as promoter (Na-Co@C). In the contrary, larger amount of CH_4 and lower selectivity to C2+ hydrocarbons and alcohols were obtained in the conventional thermal catalytic process. When using Co@C nanoparticles in the absence of Na or bare Co_3O_4 as catalyst, methane is essentially the main product (selectivity >96%). Control experiments in the presence of methanol as a hole scavenger suggest the role of light in generating charges by photon absorption via surface plasmon resonance as promoting factor. The reaction mechanism for photoassited CO_2 hydrogenation on the Co-based catalysts were investigated by near ambient-pressure X-ray photoelectron (AP-XPS) and *in situ* Raman spectroscopies, which provided information on the role of light and Na promotor in the modulation of product distribution for CO_2 hydrogenation. Spectroscopic studies suggested that surface CO_2 dissociation to CO, the stabilization of CO adsorbed on the surface of Na-Co@C catalyst and the easy desorption of reaction products is a key step for photoassisted CO_2 hydrogenation to ethanol and C2+ hydrocarbons.

Keywords

CO_2 hydrogenation, photoassisted reaction, Co nanoparticles, AP-XPS, C2+ hydrocarbons, C2+ oxygenates

Graphic Abstract

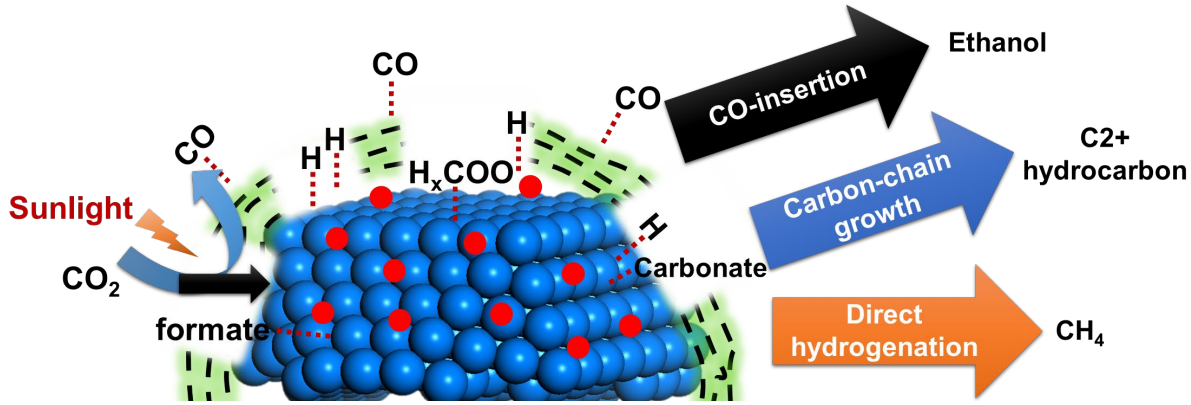

Sunlight-assisted CO_2 hydrogenation to ethanol and C2+ hydrocarbon is achieved with Na-promoted Co nanoparticles.

1. Introduction

Photocatalytic CO_2 reduction is one of the most challenging issues in chemical research.[1] In numerous investigations in this area, CO_2 reduction is coupled with the splitting of H_2O for the production of solar fuels, a process which is commonly referred to as artificial photosynthesis.[2,3] However, with heterogeneous photocatalysts, reaction rates for the transformation of CO_2/H_2O mixtures are usually in the order of micromoles per hour, which is too far from any practical application.[4-7] Moreover, the major products in most of the reports dealing with artificial photosynthesis are frequently CH_4 or CO. It appears that with the heterogeneous catalytic systems reported so far, it is very difficult to achieve carbon chain growth to go beyond CH_4 and to produce significant amounts of C2+ hydrocarbons during the photocatalytic reduction of CO_2. The formation of such light hydrocarbons is advantageous from a practical perspective due to the possibility of handling them in the liquid state.

As an alternative to the reduction of CO_2 by H_2O, in the past few years, our research group has reported the photoassisted hydrogenation of CO_2 to CH_4 on Ni (or NiO) nanoparticles under solar light irradiation.[8,9] The formation rate of CH_4 was as high as mmol/h, which is about three orders of magnitude higher than for typical CO_2+H_2O reactions. However, only CH_4 was selectively produced using Ni, NiO or other supported Group VIII catalysts.[10] In a recent work, Ozin and his co-workers reported that hydride-terminated Si nanoparticles can catalyze the reverse water-gas shift (RWGS) reaction leading to the formation of CO under photo-thermal conditions.[11] Iron nanoparticles encapsulated in carbon can also be efficient catalyst for the photoassisted RWGS reaction, as reported by Ye and co-workers.[12] However, in most of previous works, the selectivity to C2+ products are usually quite low. In a recent work, Zhang *et al.* have reported the application of CoFe@C bimetallic nanoparticles for CO_2 hydrogenation to hydrocarbons by a photothermal process.[13] In their work, it is found that, the selectivity to C2+ hydrocarbons is not affected by the light irradiation. In other words, the light irradiation only provides additional thermal energy for the reaction while does not affect the reaction mechanism. Nevertheless, the influence of solar light irradiation on the reaction mechanism for CO_2 hydrogenation is not clear.[14,15]

The lack of photoassisted processes generating C2+ hydrocarbons contrasts with conventional heterogeneous catalysis, whereby mixtures of CO_2 and H_2 can be transformed into CO or CH_4, but

interestingly, also into other C2+ hydrocarbons, depending on the catalyst.[16-20] For instance, metal nanoparticles (including Ni, Co and Ru materials) are active catalysts for CO_2 methanation, converting CO_2 to CH_4.[21-23] This reaction requires temperatures above 250 °C, giving rise to a large amount of CO (in some cases, selectivity to CO can be as high as 80%) as by-product. Moreover, metal nanoparticles (including Fe, Co and Ru materials) can also serve as active catalysts for Fischer-Tropsch (F-T) synthesis, transforming CO/CO_2 and H_2 into hydrocarbons and oxygenates, though F-T synthesis are usually performed at high pressure.[24,25] Recently, it has also been reported that Ni-NiOx nanocomposites can catalyze the CO hydrogenation into hydrocarbons by a photoassisted process.[26]

In this work, we report the photoassisted hydrogenation of CO_2 into hydrocarbons (CH_4 together with a high proportion of C2+ hydrocarbons and ethanol) using Na-promoted Co@C nanocomposites as catalysts under solar light and near-atmospheric pressure. The reaction rate of this process is in the order of mmol g_{cat}^{-1} h^{-1} and the selectivity to ethanol is 6.5% at 33% CO_2 conversion and >30% selectivity to C2+ hydrocarbons at nearly 100% CO_2 conversion. It will also be shown that the analogous thermal reaction with the same catalyst behaves differently and produces larger amounts of CH_4 and much less alcohols. The effect of light irradiation on the reaction mechanism has been studied by ambient-pressure X-ray photoelectron spectroscopy (AP-XPS) and *in situ* Raman spectroscopy. The results indicate that light has a clear effect on the formation and stabilization of intermediates for the production of ethanol and the C-C chain growth process for the production of C2+ hydrocarbons.

2. Results and discussion

2.1 Synthesis and structural characterization of Na-promoted Co@C

Na-promoted Co@C nanocomposites (denoted as Na-Co@C) were prepared by thermal decomposition of cobalt-sodium-ethylenediaminetetraacetate (Co-Na-EDTA) complexes at 450 °C (see Experimental section below) in H_2 atmosphere.[27] As shown in **Figure S1**, the X-ray diffraction (XRD) pattern of this sample only shows the diffraction peaks corresponding to metallic cobalt, being ***fcc*** (PDF code: 96-900-8467) and ***hcp*** phases (PDF code: 96-900-8493) as the predominant and minor phases present, respectively. Moreover, the Raman spectrum (see **Figure S2**) reveals that

CoO_x species (Co_3O_4) are also detectable in the sample together with disordered carbon. To gain further understanding on the structure of Na-Co@C, the sample was studied by electron microscopy. As shown in **Figure 1a-b**, Na-promoted Co@C nanocomposites consist of nanoparticles with sizes ranging from 10 to 100 nm. The high-resolution transmission electron microscopy (HRTEM) images in **Figure 1c** and **1d** show that Co nanoparticles are surrounded by thin carbon layers. Lattice fringes corresponding to metallic Co and Co_3O_4 can be observed in this sample, suggesting that, either part of the Co^{2+} species maintained their oxidation state, or part of the metallic Co was oxidized when exposed to air after the preparation. It is interesting to note that the core of the nanoparticles consisted of metallic cobalt, whereas Co_3O_4 patches are present on their surfaces below the carbon layers. Due to the presence of thin carbon layers, Co nanoparticles are protected from deep oxidation by air. Elemental mapping indicates that Co, C, O as well as Na are regularly dispersed in the nanocomposites **(Figure 1f-j)**. The Na-Co@C sample contains *ca.* 95 wt.% of Co and ~2 wt.% of Na. An analogous Co@C sample free of Na has been also prepared (see the experimental section for synthesis procedure).[28] Similar to the Na-promoted sample, HRTEM shows the presence of Co nanoparticles surrounded by thin carbon layers (see **Figure S3**), with CoOx patches on the surface and metallic Co as the core. The XRD pattern of the Co@C sample is also similar to Na-Co@C, showing the typical diffraction pattern of ***fcc*** metallic Co and a small proportion of ***hcp*** Co.

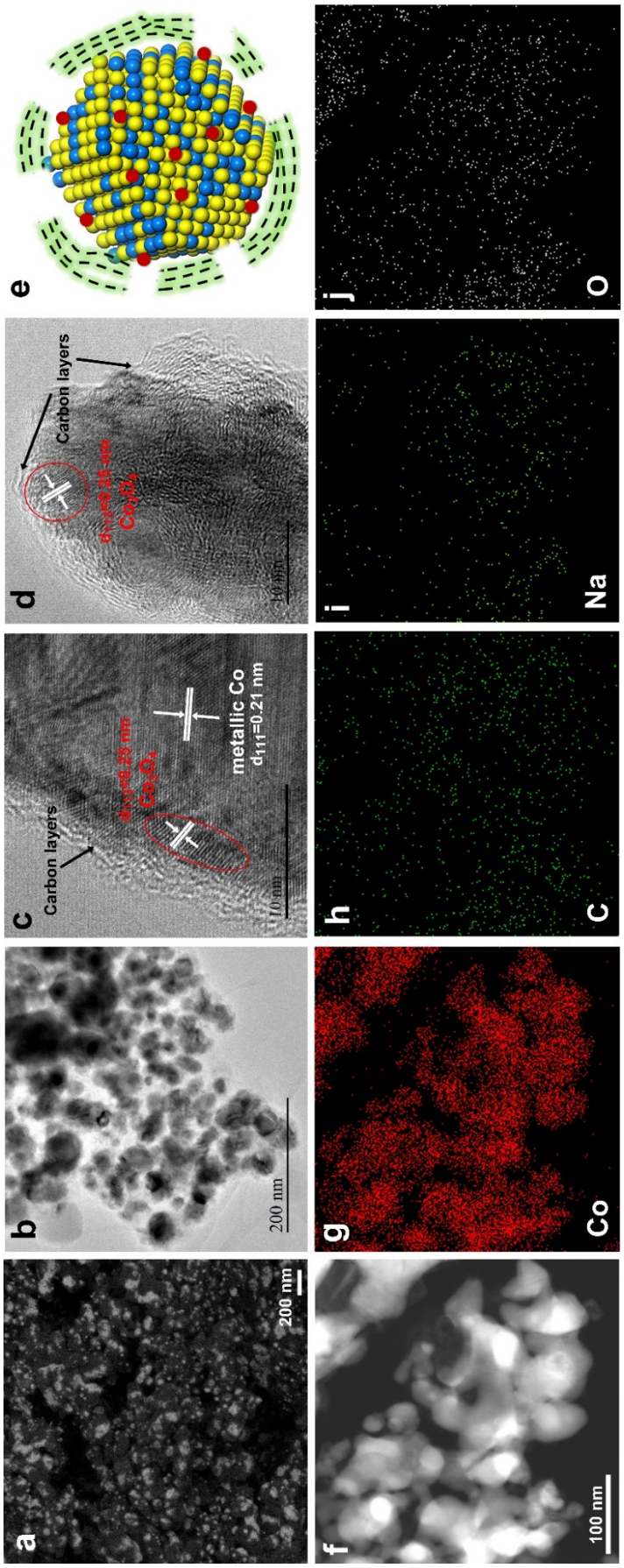

Figure 1. Structural characterization of Na-Co@C sample. (a) Field-emission scanning electron

microscopy (FESEM) image, (b) transmission electron microscopy (TEM) images, and (c, d) high-resolution transmission electron microscopy (HRTEM) images of Na-Co@C sample. (e) A schematic illustration of one Na-Co@C nanoparticle. Co, CoO_x and sodium are represented by yellow, blue and red balls, respectively, while the carbon layers are represented as shaded dashed lines. (f) Scanning transmission electron microscopy (STEM) image and (g-j) corresponding elemental mapping of different elements in the Na-Co@C sample.

2.2 Photoassisted CO_2 reduction

Table 1. Sunlight-assisted and thermal CO_2 hydrogenation on different cobalt catalysts.

Sample	Conversion/%	Selectivity[c]/%								
		CH_4	CO	Ethanol	C2	C3	C4	C5	C6	Other products
Na-Co@C-photothermal[a]	97.0	62.7	-	0.6	16.5	12.5	4.8	2.0	0.6	0.3
Co@C-photothermal[a]	98.8	92.6	-	-	4.4	1.8	0.7	0.3	0.1	-
Co_3O_4-photothermal[a]	96.9	98.6	-	-	1.4	-	-	-	-	-
Na-Co@C-thermal[b]	91.5	67.4	-	0.4	11.9	10.4	5.1	2.7	1.3	0.6

[a] Reaction conditions for photoassited CO_2 hydrogenation reaction: mixture of CO_2 (20 mL), H_2 (100 mL), and N_2 (20 mL); catalyst mass, 75 mg; irradiation source, solar simulator. Blank controls in the absence of any solid catalyst or the reaction in the dark without heating did not lead to any product. The temperature of the sample (235 °C) under the photothermal conditions was measured by a thermocouple placed in close contact with the upper surface of the powdered solid. [b] The thermal reaction was performed at the same temperature as the photothermal process without the presence of solar light irradiation. [c]The selectivity to different products are normalized to carbon.

The performance of three Co-based nanoparticulate catalysts for the photoassisted reaction of CO_2+H_2 under simulated sunlight is shown in **Table 1**. For comparison, the photoassisted activity of commercial Co_3O_4 nanoparticles supplied by Sigma-Aldrich (the TEM images of commercial Co_3O_4 nanoparticles are shown in **Figure S4**) and Co@C nanoparticles (without Na) was also measured under the same conditions. As can be seen (**Table 1, entry 3**), Co_3O_4 was able to catalyze the hydrogenation of CO_2, and CH_4 was the major product (>98% selectivity). In the case of Co@C

catalyst, CH_4 also appeared as the dominant product and low selectivity to ethane (4.4%) was also observed. When Na-Co@C was used as the catalyst (**Table 1, entry 1**), CH_4 selectivity was markedly lower (62.7 %), and more importantly, C2+ hydrocarbons and ethanol were also formed. These results suggest that the presence of Na is crucial for the production of C2+ hydrocarbons during the photoassisted hydrogenation of CO_2, which is in line with classic heterogeneous catalytic systems favoring the formation of hydrocarbon chains.[29] We also tested Na-Co@C under thermal conditions without sunlight irradiation at the same temperature measured under photoassisted conditions (235 °C). As shown in **Table 1**, the selectivity to C2+ hydrocarbons is lower than that obtained under photothermal conditions and a small amount of ethanol is also observed at high CO_2 conversion.

It has been claimed that solar light irradiation can increase the temperature of the catalyst surface by plasmonic effects, which further enhance the activity while does not influence the selectivity.[12,13] In our case, we have also tested the Na-Co@C catalyst for CO_2 hydrogenation under photothermal conditions at different temperature. As shown in **Figure S5**, at similar CO_2 conversion (>97%), the selectivity to C2+ hydrocarbons decreased with the temperature and more CH_4 was produced at higher temperature, suggesting that the improved selectivity to C2+ hydrocarbons is not caused by the thermal effects under the photothermal conditions.

Since various of products were observed on Na-Co@C sample under both photothermal and thermal conditions, the product distributions obtained at different CO_2 conversion were followed and given in **Figure 2**. Under both photothermal and thermal conditions, the small amounts of CO formed initially were gradually consumed, and eventually could not be observed among the products (see **Figure 2a** and **Figure 2b**). This leads to conclude that CO was produced as a reaction intermediate, which then evolved towards the formation of higher hydrocarbons and alcohols through CO dissociation or a CO insertion mechanism respectively.[30] Notably, the selectivity to CO under photothermal conditions is slightly higher than under thermal conditions while selectivity to CH_4 is lower under photothermal conditions.

Furthermore, the variations of hydrocarbons and ethanol along the CO_2 hydrogenation were also followed. As presented in **Figure 2c**, under photothermal conditions, the selectivity to ethanol and C2+ hydrocarbons is 6.5% and 36.3% respectively, when the CO_2 conversion is 33%. With the

increase of CO_2 conversion, the selectivity to ethanol decreases. According to the catalytic results, the chain growth probability factor (α) for hydrocarbon result in 0.55 at 37-58% CO_2 conversion and decreases to 0.38 at 97% CO_2 conversion.

It is clearly shown that, the yield of ethanol (<0.8%) on Na-Co@C sample under thermal conditions is significantly lower than under photothermal process. Nevertheless, the selectivity to light olefins is also lower under thermal conditions (see **Table S1 and Table S2** in supporting formation). In the thermal process, the chain growth probability factor α is ~0.55 at all CO_2 conversion, which is similar to values reported in the literature for the CO_2 hydrogenation on cobalt-based catalysts.[31] The above catalytic results clearly indicate that, the solar light irradiation has significant influences on the product distribution during CO_2 hydrogenation. With the help of sunlight irradiation, the selectivity to C2+ hydrocarbons and ethanol is promoted, especially at medium CO_2 conversion (<50%).

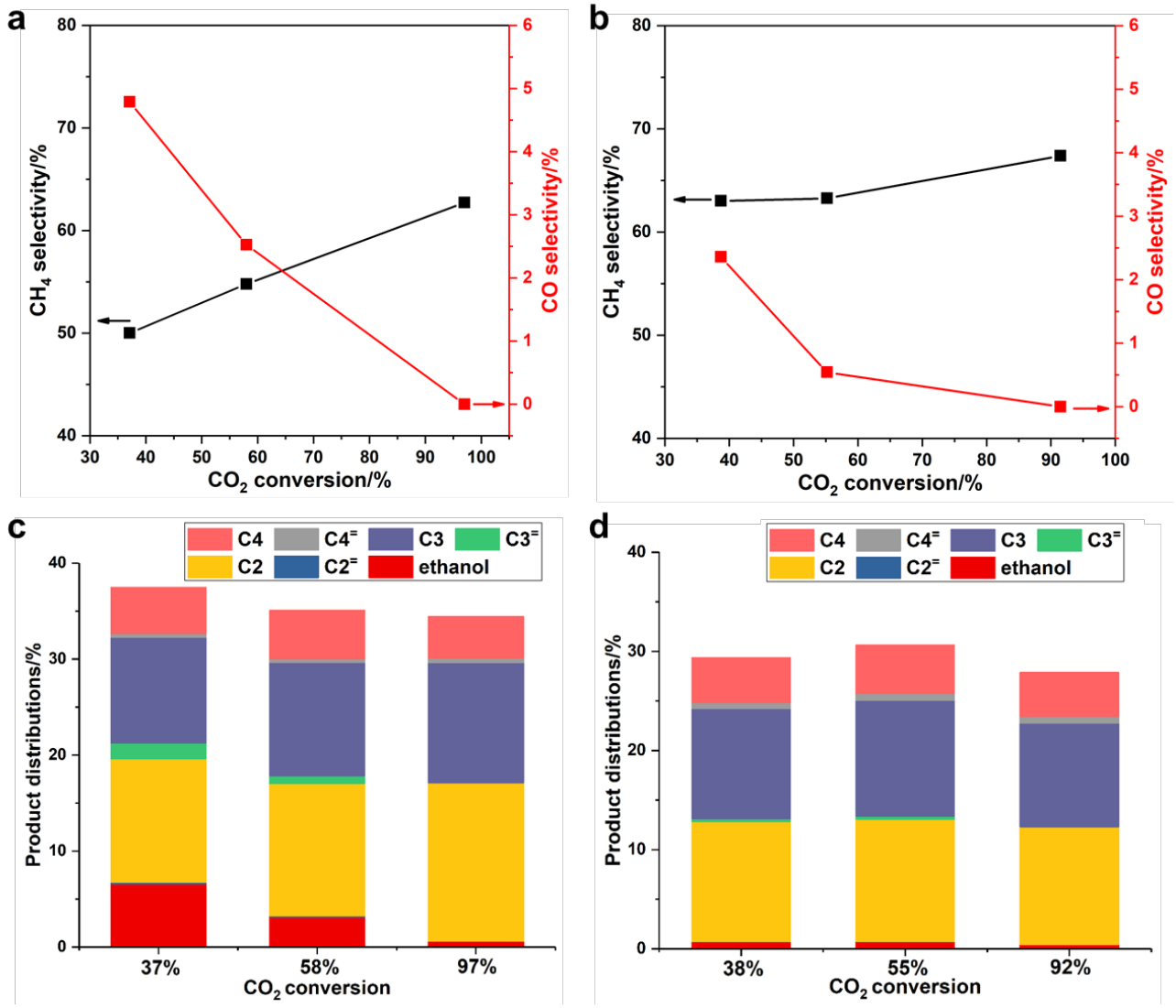

Figure 2. Evolution of the products during CO_2 hydrogenation with Na-Co@C under photothermal and thermal conditions. (a) Selectivity to CH_4 and CO at different CO_2 conversion under photothermal conditions at different CO_2 conversion. (b) Selectivity to CH_4 and CO at different CO_2 conversion under thermal conditions at different CO_2 conversion. (c) Selectivity to C2+ hydrocarbons and ethanol under photothermal conditions at different CO_2 conversion. (d) Selectivity to C2+ hydrocarbons and ethanol under thermal conditions at different CO_2 conversion.

2.3 Effect of light on the catalytic performance

In previous works, it has been reported that CO_2 hydrogenation can be enhanced under solar light irradiation.[12,32] Herein, we have also observed that the initial reaction rate of the CO_2 hydrogenation on Na-Co@C under thermal conditions was lower than for the analogous process performed under

photothermal conditions (see **Figure S6**). The Na-Co@C nanomaterials show an intense light absorption profile throughout the entire UV-vis spectrum (see **Figure S7**). In order to investigate on which wavelengths might be responsible for the activation of CO_2 hydrogenation, irradiations were performed using monochromatic light of selected frequencies (see **Figure S8**). Light in the UV range (<400 nm), coincident with the expected surface plasmon resonance of metallic cobalt nanoparticles, was observed to promote the reaction in a noticeable way.[33] Therefore, it can be deduced that photo-generation of charges (electron-hole pairs) on Co nanoparticles might participate in the CO_2 hydrogenation reaction. A recent study on the use of carbon-coated iron nanoparticles in a similar process suggested that hot electrons generated by absorption of UV light were responsible for activating CO_2.[12]

In the present system, we considered the hypothesis of direct participation of the photo-generated charges, which would be transferred to appropriate adsorbed species and then involved in CO_2 hydrogenation reaction. Therefore, control experiments by adding a hole scavenger in the reaction system were designed to check whether consumption of photo-generated charges had any effect on activity. A series of sunlight-assisted experiments in the absence or in the presence of methanol as a hole scavenger were performed (see **Figure S9**). The introduction of a small amount of methanol vapor in the cell leads to a slight decrease in the initial reaction rates. A further increase in the amount of methanol leads to a significantly greater decrease of the initial activity. Based on the aforementioned evidences, it is proposed here that the photoassisted CO_2 hydrogenation on Na-Co@C nanocomposites is to some extent activated by the UV light.

3. Mechanistic studies based on *in situ* spectroscopy

Due to the complexity of the CO_2 hydrogenation reaction, molecular characterizations of the catalyst under working conditions at molecular level have been carried out to identify the nature of active sites and establish correlations between structure and catalytic reactivity. Thus, near-ambient pressure X-ray photoelectron spectroscopy (AP-XPS) and *in situ* Raman studies have been performed providing useful information on the nature of surface intermediate species involved in the reaction mechanism and the chemical states of the catalyst surface in the presence of CO_2/H_2 mixture. A detailed analysis of surface species under reaction conditions will allow to shed light on the role of light irradiation and the promoting effect of sodium on the catalytic behavior of Na-Co@C sample for CO_2 hydrogenation.

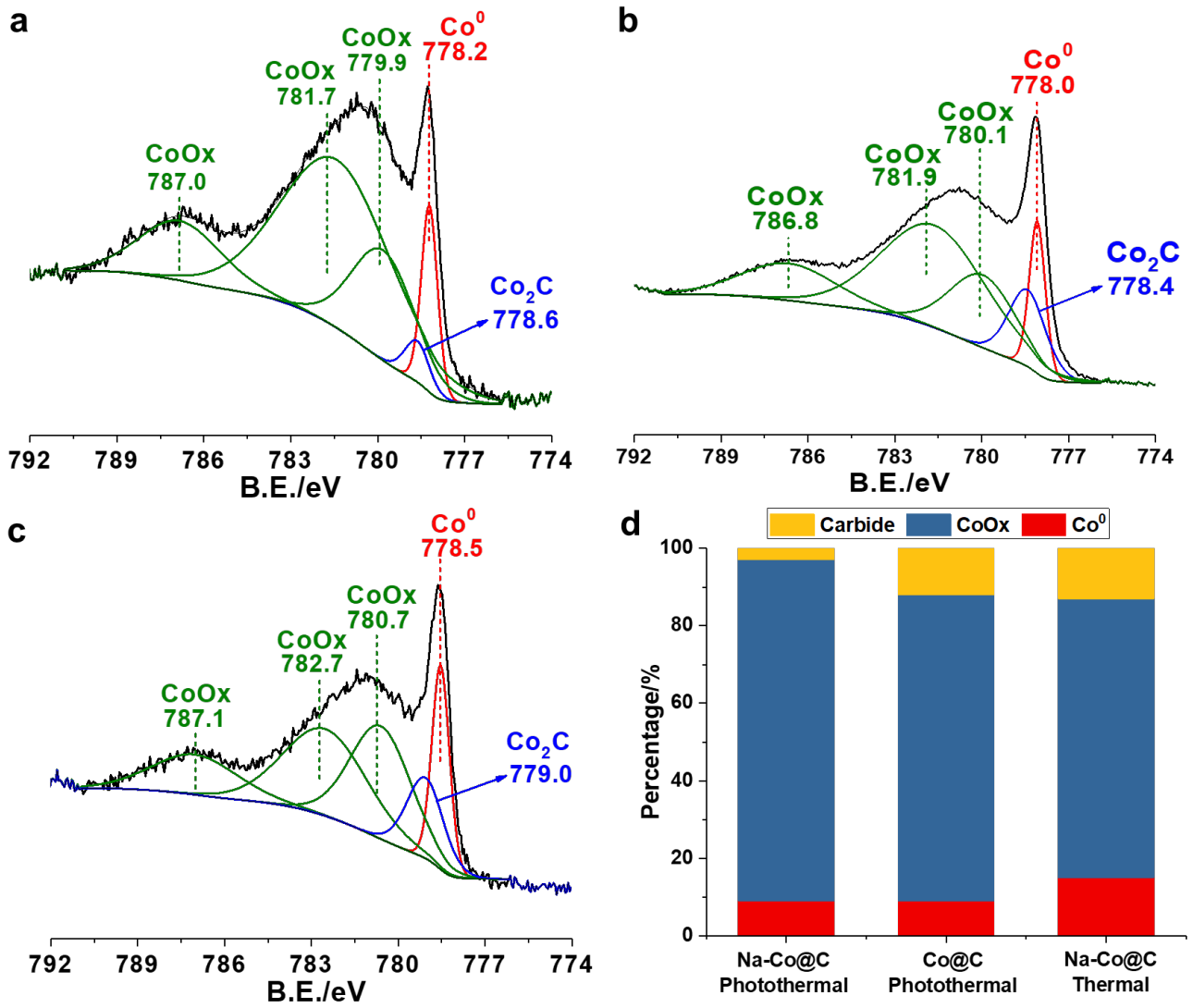

Figure 3. AP-XPS spectra of Co2p$_{3/2}$ region obtained at 250 °C with incident X-ray energy of 1000 eV. (a) Na-Co@C under photothermal conditions, (b) Co@C under photothermal conditions and (c) Na-Co@C under thermal conditions. (d) Percentage of cobalt carbide, CoOx and metallic Co^0 in different Co-based catalysts based on the AP-XPS spectra.

3.1 AP-XPS studies on the surface properties of Co-based catalysts

In contrast to the Na-Co@C sample, a different catalytic behavior has been observed on the Na-free Co@C sample under photoassited reaction conditions (see **Table 1**). The role of sodium in FTS cobalt based catalysts has extensively been discussed in the literature. It has been proposed that sodium can stabilize cobalt carbide species which serve as active sites for the formation of oxygenates.[34,35] In some other works, it is suggested that cobalt carbides can suppress the

hydrogenation of C=C bonds and facilitate the desorption of olefins, leading to higher selectivity to olefins.[36] However, it has also been proposed that cobalt carbides can decrease the reducibility of cobalt oxide and/or block active sites, resulting in lower catalytic activity for FTS.[37,38]

As shown in **Figure 3a**, carbide species have been detected on the Na-Co@C sample in the $Co2p_{3/2}$ spectra under light irradiation. At the reaction temperature (250 ºC), Co2p3/2 peak fitting shows the co-existence of Co^0 (9%), CoO (88%) and Co_2C (3%) species. Notably, the formation of carbide species is rather low, leading us to question their participation in the formation of alcohols under our reaction conditions. The low reducibility of cobalt species under reaction conditions should also be noted. On the other hand, under light irradiation and in the absence of Na, Co2p3/2 peak fitting shows the presence of Co^0 (9%), CoO (79%) and Co_2C (12%) at 250 ºC (**Figure 3b**). A higher amount of cobalt carbide is observed on the Co@C sample while the amount of metallic Co is similar to Na-Co@C sample, implying that the promotion effect of Na does not seem to relate with either the increase of reducibility or stabilization of carbide. Nevertheless, the $Co2p_{3/2}$ peak fitting of the Na-Co@C sample under thermal condition (see **Figure 3c**) shows the presence of Co^0 (15%), CoO (72%) and Co_2C (13%), suggesting that sunlight irradiation can suppress the formation of cobalt carbide.

The abovementioned XPS results of $Co2p_{3/2}$ region indicate that, higher selectivity to C2+ hydrocarbons and ethanol on Na-Co@C sample under photothermal conditions is probably not related with cobalt carbide species. Moreover, considering the similar percentage of metallic Co in the above three cases, it seems that the observed different catalytic behavior is not related with the reducibility of the Co catalyst.

3.2 AP-XPS studies on the surface carbon species

Though several reaction paths have been proposed for the CO_2 hydrogenation reaction, the starting point is the activated $CO_2^{\delta-}$ specie which can either dissociate into CO+O or undergo direct hydrogenation.[39] The *in situ* formed CO can be further hydrogenated or dissociate into C and O ad-atoms, resulting in the formation of different surface species, like for instance formyl (HCO), hydroxycarbene (HCOH), hydroxymethyl (H_2COH), methyl (CH_3), methylene (CH_2), methylidyne (CH) and hydroxymethylidyne (COH). Chain growth takes place by a surface polymerization

condensation reaction process resulting in the formation of paraffin's, olefins and oxygenates. The types of the surface carbon species can be used as fingerprint for reaction pathways towards different products. Therefore, we firstly have studied the surface carbon species by AP-XPS to follow their evolution on Co-based catalysts.

The C1s and $Co2p_{3/2}$ XPS peaks of the Na-Co@C and Co@C samples in presence of CO_2 and H_2, under thermal and photothermal reaction conditions, are shown in **Figure 4** to **Figure 6**, where XPS spectra have been acquired at two X-Ray energies, 510 eV and 1000 eV, in order to analyze at different depths of the sample. Firstly, the Na-Co@C sample has been studied. The C1s spectra (**Figure 4a-4c**) under light irradiation and working at 510 eV X-Ray energy, show predominately CO (BE 286.5 eV) as main component in addition to formate (BE 287.8 eV) and carbonate species (BE 289.4 eV).[40-42] When working at higher X-Ray energy (1000 eV) (**Figure 4e-4g**), besides CO (BE 286.5 eV), formate (287.4 eV) and carbonate species (290.2 eV), an additional component at 288.6 eV is observed. In the O1s region (**Figure S10a**), a new component at 532.8 eV appears when increasing the reaction temperature, showing similar behavior to the C1s component at 288.6 eV. Based on the high BE of both species and their parallel growing, we can tentatively assign both components to some type of hydrogen-carbonate intermediate specie, i.e HxCOO*. Peak areas of each component according to the fitting results of C1s spectra, and their evolution as a function of the temperature, are given in **Figure 4d** and **Figure 4h**. Taking into consideration that CO is predominantly observed at low X-Ray energy (being high surface sensitive conditions) and Co nanoparticles are covered by thin carbon layers, the XPS results indicate that CO is stabilized on the surface carbon layers of the Na-Co@C sample. At higher X-Ray energy (1000 eV), the contribution of formate and HxCOO* in the C1s peak increases, indicating their stronger interaction with Co surface covered by the carbon layers. Based on **Figure 4d and 4h**, it can be observed that when increasing reaction temperature, the signal intensity of the surface CO decreases, while formate species and the component at 288.6 eV increase. Meanwhile carbonate like species remains practically stable with the temperature. This behavior indicates that CO, formate and HxCOO* behave as intermediate species while carbonate species, stabilized either on cobalt surface or on the carbon layer, are not involved in the reaction pathways.

The CO_2 hydrogenation on Na-Co@C sample under thermal conditions has also been studied by

AP-XPS. As shown in **Table 1** and **Figure 2**, the product distribution under thermal conditions with Na-Co@C for CO_2 hydrogenation is similar to the situation under photothermal conditions, although selectivity to C2+ hydrocarbons and ethanol were lower under thermal conditions. Based on the AP-XPS studies (**Figure 5a-5c**), CO (BE 286.7 eV) is not detected on the catalyst surface under thermal conditions, while it is detected in the gas phase (**Figure S11**), suggesting that CO interacts weakly with the catalyst surface under thermal conditions. Since the stabilization of CO on catalyst surface is a key for the formation of oxygenates during CO_2 hydrogenation, the absence of CO on Na-Co@C under thermal conditions can explain its low selectivity to ethanol. Besides, Carbonate (290.5 eV), Formate (287.1 eV) and HxCOO*, are also predominately observed in the C1s spectra. Notoriously carbide species with BE 283.7, 281.6 eV (also observed in the Na-Co@C sample under light irradiation) and graphitic carbon species and/or CHx species with BE at 284.9 eV are also detected, which is in line with the higher amount of cobalt carbide as observed in **Figure 3**.

Considering our previous hypothesis where UV light plays an important role in the CO_2 activation through the formation of electron hole pairs, a support for this hypothesis can be found from the AP-XPS studies. In the AP-XPS studies, two C1s peaks at 285.2-285.6 and 284.1-284.7 eV have been observed in the sample under light irradiation (**Figure 4**). The first ones correspond to carbon as observed in the sample without irradiation, while the second one is only observed on irradiated samples. The low BE of the C1s peak at 284.1-284.7 eV may account for electron-rich carbon species from the carbon layer formed under light irradiation, which play an important role in the activation of CO_2 to $CO_2^{\delta-}$, enhancing the CO_2 dissociation to CO and O.

In order to explain the ~92% CH_4 selectivity observed in the Co@C catalyst, and in an attempt to find out why and how Na plays an effect of the product distribution, the evolution of carbon intermediate species at different reaction temperatures has been followed by AP-XPS studies (**Figure 6**). Surprisingly, a different reaction intermediate is observed in the non-promoted Co@C catalyst, where a new component at 288.2 eV, not observed in the Na-Co@C sample, is predominant. In addition, CO (BE 286.5 eV) is also formed together with surface carbonate species (BE 290.5 eV). Formate species (BE 287.4 eV) are only detected at low temperature (**Figure 6a-c**). Based on the growth of a parallel new component at 530.6 eV in the O1s peak (**Figure S10b**), associated to hydroxyl groups, we can assign the peak at 288.2 eV to enol like species (HxCOH). These enol like

species are unstable on Co surface, and further C-OH scission would lead to formation of CHx species, which can be further hydrogenated into CH_4, as detected in the catalytic studies.

Combining the above AP-XPS results, it can be concluded that, under light irradiation, the promoting effect of sodium on the production of C2+ hydrocarbons and oxygenate cannot be ascribed to any of the effects described previously in the literature.[43-45] The effect of Na in our system is probably related with the modulation of the surface intermediates during the catalytic process of CO_2 hydrogenation, resulting in different product distributions. Meanwhile, we have observed that light plays an important role in the reaction mechanism, by modulating the types of intermediates species and their stability (especially CO) on the surface of Co nanoparticles.

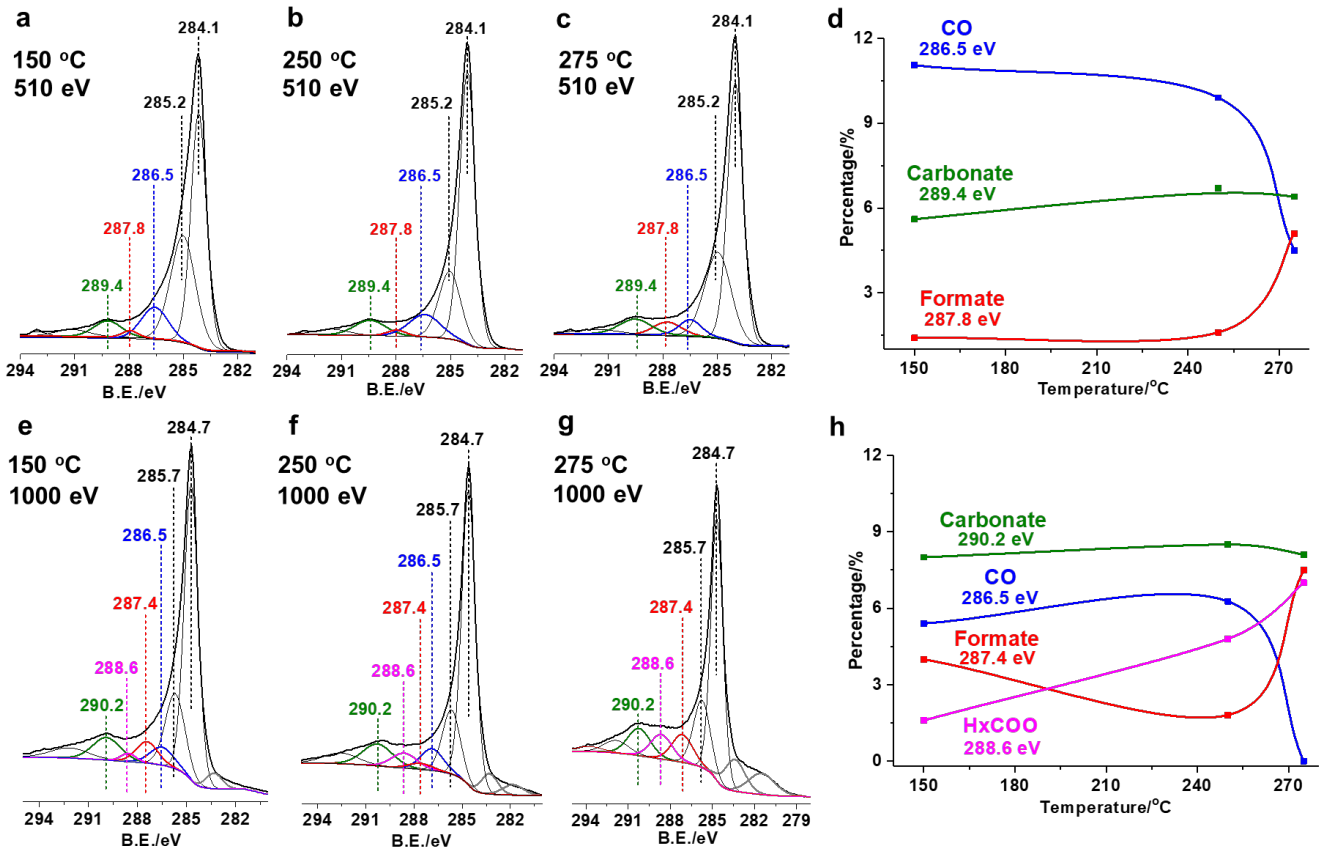

Figure 4. Ambient-pressure XPS spectra of Na-Co@C catalyst for CO_2 hydrogenation under photothermal conditions. (a-c) C1s spectra obtained with incident X-ray energy of 510 eV. (d) Percentage of different types of carbon species at different temperature according to the spectra obtained at 510 eV. (e-g) Spectra obtained with incident X-ray energy of 1000 eV. (h) Percentage of different types of carbon species at different temperature according to the spectra obtained at 1000

eV.

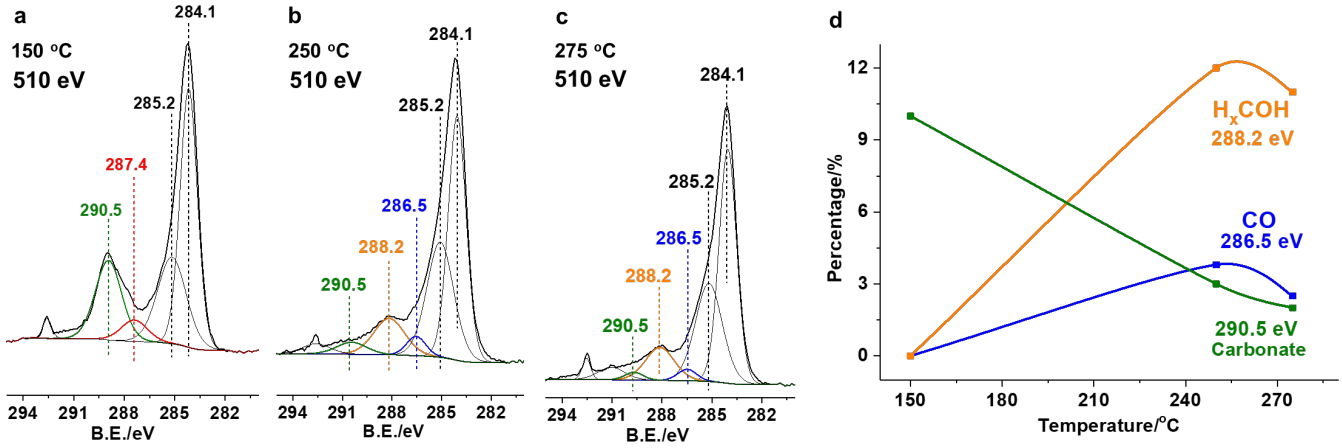

Figure 5. (a-c) C1s AP-XPS spectra of Co@C sample under photothermal conditions obtained with incident X-ray energy of 510 eV. (d) Percentage of different types of carbon species at different temperature according to the spectra obtained at 510 eV.

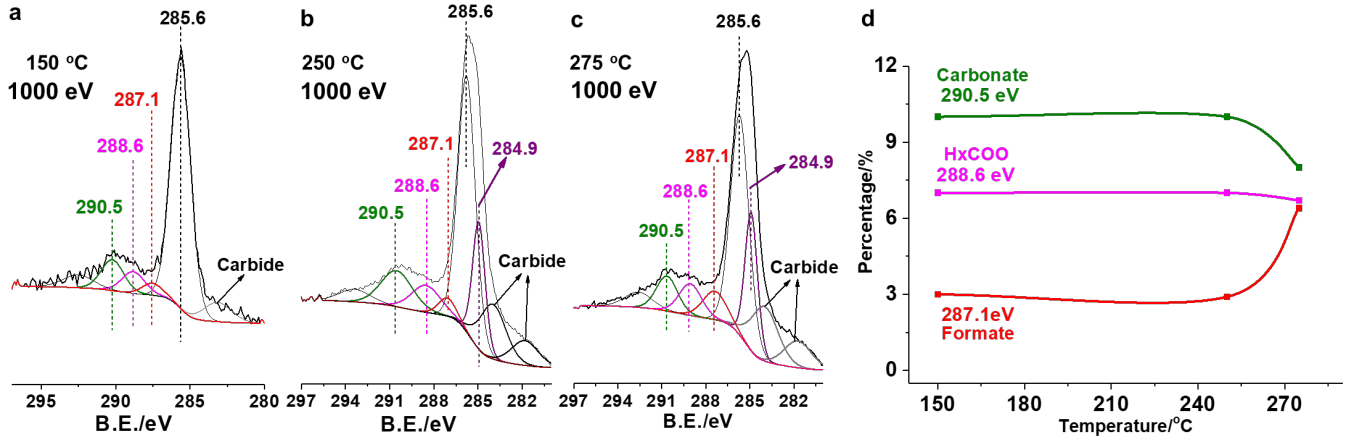

Figure 6 (a-c) C1s AP-XPS spectra of Na-Co@C sample under thermal conditions obtained with incident X-ray energy of 1000 eV. (d) Percentage of different types of carbon species at different temperature according to the spectra in obtained at 1000 eV.

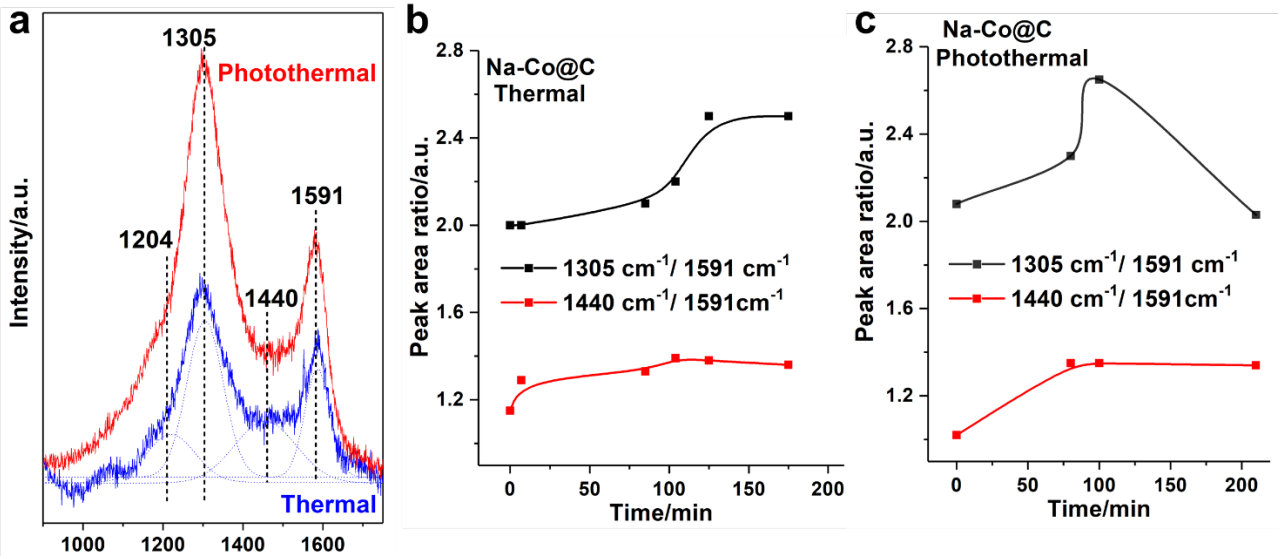

Figure 7. *In situ* Raman spectra of Na-Co@C under thermal and photothermal conditions for CO_2 hydrogenation. (a) Raman spectra obtained with Na-Co@C sample after 100 min reaction under photothermal (red curve) and thermal (blue curve) conditions for CO_2 hydrogenation. (b) Peak area ratio of the Raman bands at different reaction time under photothermal and thermal conditions for CO_2 hydrogenation.

3.3 *In situ* Raman Studies on the surface carbon species

The formation of carbon species in the CO_2 hydrogenation process, already detected in the AP-XPS studies. As shown before in **Figure 3**, the amount of cobalt carbide formed on Na-Co@C under thermal conditions is more than under photothermal conditions. The high sensitivity of Raman spectroscopy to carbonaceous species, and the possibility to work under more realistic reaction conditions (1 bar in Raman versus 1 mbar in AP-XPS) enables us to obtain more realistic information about the formation of carbon species and their evolution under operando conditions.

Peak fitting of the Raman spectra of the Na-Co@C catalyst, shows several bands at 1204, 1305, 1440 and 1591 cm^{-1} associated to different carbon species (see **Figure 7**), which can be ascribed to disordered graphite, capillary carbon or defects in graphite, amorphous carbon and graphite like carbon, respectively.[46,47] Under thermal CO_2 hydrogenation conditions, an increase in the amount of amorphous carbon (1.15 to 1.39) and capillary carbon (2.08 to 2.5) is observed with reaction time. Under photothermal conditions, the amount of capillary carbon species increases in the first 100 min

from 2.08 to 2.65 and then decreases to 2.03, while amorphous carbon increases and remains practically constant (1.02 to 1.35). Thus, the *in situ* Raman results infer that sunlight irradiation suppress the carbon deposition on Na-Co@C catalyst. Such effect may cause the low percentage of cobalt carbide formed on the Na-Co@C catalyst under photothermal conditions.

4. Influence of sunlight irradiation on the structure of the Co-based catalysts

The morphologies of Co-based catalysts after CO_2 hydrogenation reactions under thermal and photothermal conditions have been studied by TEM. As shown in **Figure S12**, the morphology of Na-Co@C after photothermal and CO_2 hydrogenation is different to the pristine sample. Rod-like structures are formed along the spherical Co nanoparticles. Elemental mapping (see **Figure S13**) results show that, those rod-like structures contains Co, suggesting that structural reconstruction occurred during the CO_2 hydrogenation reaction under photothermal conditions. Furthermore, HRTEM images indicate that, those rod-like structures corresponding to Co_3O_4. However, those Co_3O_4 species may come from the re-oxidation of metallic Co^0 or Co_2C species after contact with air during preparation of the samples for TEM measurements. Besides, we have also measured the other Co catalysts after CO_2 hydrogenation reactions. As shown in **Figure S14** to **Figure S16**, rod-like structures can be observed in all the cases, suggesting the structural reconstruction is a common phenomenon in Co catalysts for CO_2 hydrogenation reaction. Catalyst reconstruction could be also reflected from the AP-XPS data where the number of exposed cobalt surface sites increases under reaction conditions (**Table S3**). It should be noted that, the size of the rod like structures formed in Co_3O_4 nanoparticles are larger than those formed in either Na-Co@C or Co@C. According to the literature, CH_4 is more favorable to form on larger Co crystallites.[48,49] The very high selectivity (98.6%) to CH_4 on Co_3O_4 under photothermal conditions may be related with the large Co particle size formed under reaction conditions.

In addition, in conventional Fisher-Tropsch processes, the presence of the Co^0 ***hcp*** phase plays an important role during the growth of carbon chain for producing higher hydrocarbons.[50,51] As shown in **Figure S17**, the percentage of the Co^0 ***hcp*** phase increases significantly in the Na-Co@C sample after the photoassisted reaction. For comparison purposes, the XRD pattern of the Na-Co@C sample after only-thermal catalytic hydrogenation of CO_2 was also measured. The percentage of ***hcp*** phase

Co also increased in this case, but not as much as after the photoassisted reaction, implying that solar light irradiation during the CO_2 hydrogenation reaction can promote the transformation of Co species into the ***hcp*** phase, which may have influence on the catalytic behavior, especially on the selectivity to ethanol and C2+ hydrocarbons.

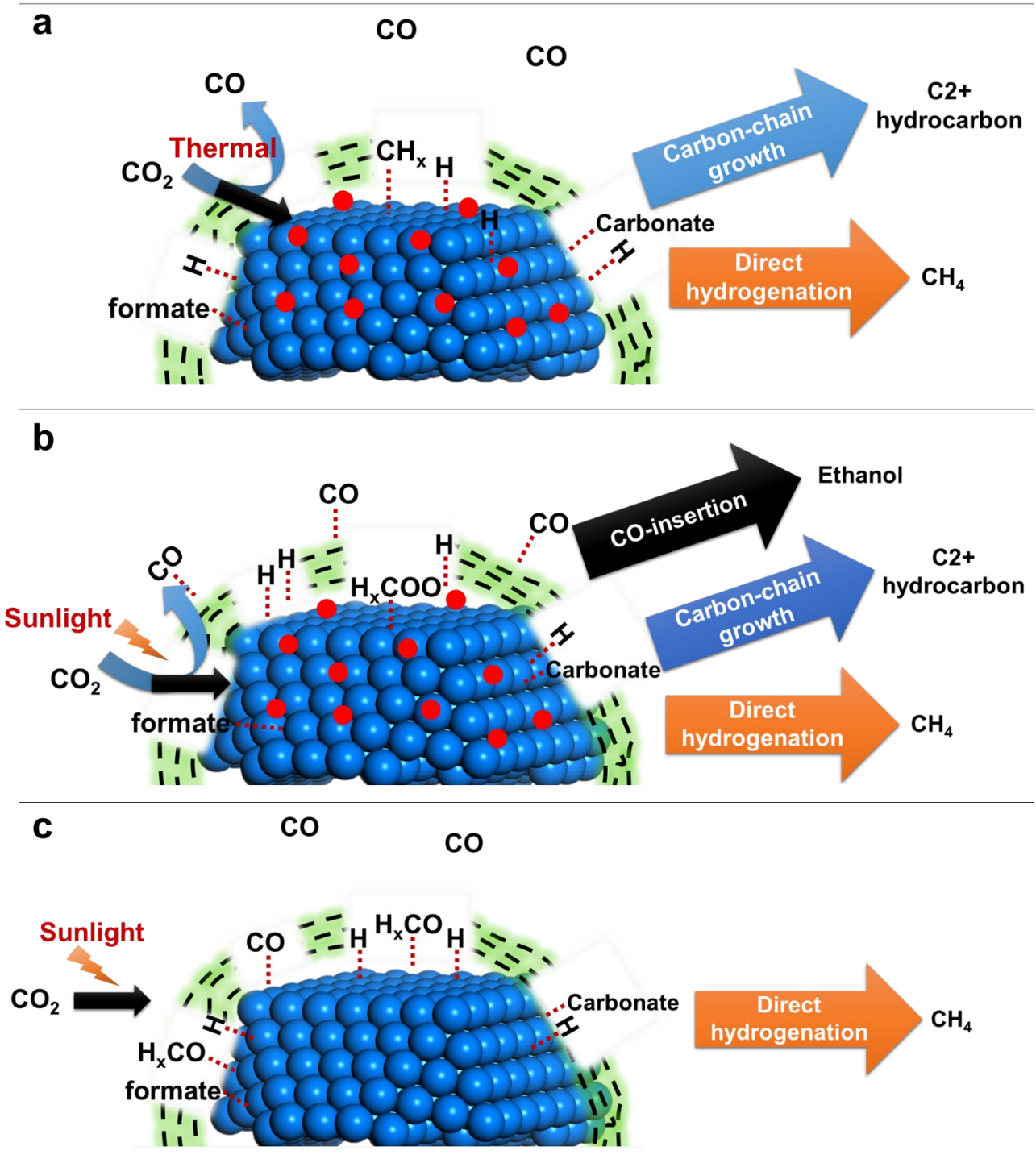

Figure 8. Schematic illustration of the CO_2 hydrogenation on Na-Co@C and Co@C catalysts under

thermal and photothermal conditions. Sodium is shown with red circles. (a) Under thermal conditions, Na-Co@C catalyst mainly produce CH_4 and C2+ hydrocarbons. (b) Under photothermal conditions, ethanol is also produced as well as C2+ hydrocarbon and CH_4. (c) Under photothermal conditions, CH_4 is the predominant product on Co@C sample, due to the fast hydrogenation of the intermediates instead of C-C coupling reaction.

5. Proposed reaction mechanism

Based on the above spectroscopic studies, we can conclude that light irradiation plays an important role in the CO_2 activation mechanism, favoring the RWGS reaction ($CO_2 + H_2 \rightarrow CO + H_2O$) and the stabilization of CO on the catalyst surface. The direct role of light has been ascribed to an electronic effect where electrons generated by absorption of UV light are responsible for activating CO_2 to $CO_2^{\delta-}$, promoting CO_2 dissociation into CO, and the stabilization of CO on the catalyst surface. The stabilization of CO contributes to a higher selectivity toward ethanol by a CO insertion mechanism. Moreover, a clear effect of light on the chain growth process can also be deduced according to the different surface intermediates observed by AP-XPS. This can be reflected from the catalytic results where under light irradiation the ASF hydrocarbon distribution differs from the thermal process, with a higher selectivity to C_2H_6 and C_3H_8 and ethanol. The higher selectivity to C_2H_6 and C_3H_8 under light irradiation can be related to a lower concentration of surface C species, or to low metal-C adsorption strength promoting hydrocarbon desorption. At this point, and based on our spectroscopic data, it has been observed that sunlight irradiation can reduce the metal-carbon interaction. Indeed, the amount of carbide species observed in the AP-XPS spectra is markedly lower in the presence of light than under thermal conditions. Nevertheless, we have also observed the influence of light irradiation on the phase structure of Co catalysts, which show higher amount of Co ***hcp*** phase under sunlight irradiation. Finally, and in agreement to literature data, sodium plays an important role on the C-C formation by influencing the nature of intermediate species on the catalyst surface. In the absence of sodium, enol species seem to be stabilized, and the C-OH scission favors the formation of CH_4.

6. Conclusions

In summary, we report the application of Na-Co@C nanocomposites for photocatalytic hydrogenation of CO_2 to C2+ hydrocarbons and ethanol. Under photoassisted conditions the Na-promoted Co@C sample shows almost 100% selectivity to hydrocarbons as well as high selectivity to C2 and C3 products (16.5% and 12.5% respectively) at >97% CO_2 conversion. Photo-generation of charges on metallic Co nanoparticles via surface plasmon resonance effect upon UV light absorption, in addition to the favored formation of active ***hcp*** phases under such conditions, proved the activating role of sunlight irradiation in the photoassisted process. Control experiments confirm the participation of photo-generated charges in the catalytic process. In addition, AP-XPS studies have shown a direct role of light irradiation on the formation of electron rich carbon species on the surface of Na-Co@C nanoparticles. These species are involved in CO_2 activation to $CO_2^{\delta-}$, promoting CO_2 dissociation into CO. Moreover, CO is stabilized by interaction with the carbon layers on the catalyst surface, enabling the formation of ethanol via a CO insertion mechanism. Based on spectroscopic studies, this work shows how the light irradiation can influence the surface intermediate species during CO_2 hydrogenation reaction, leading to different reaction pathways.

ACKNOWLEDGEMENTS

L.L. thanks ITQ for providing a contract. A.V.P. thanks the Spanish Government (Agencia Estatal de Investigación) and the European Union (European Regional Development Fund) for a grant for young researchers (CTQ2015-74138-JIN, AEI/FEDER/UE). The authors also thank the Microscopy Service of UPV for kind help on FESEM, TEM and STEM measurements. Financial supports from the Spanish Government-MINECO through “Severo Ochoa” (SEV-2016-0683) program are also gratefully acknowledged.

References

1 G. A. Ozin, *Adv. Mater.*, 2015, 27, 1957-1963.
2 N. S. Lewis and D. G. Nocera, *Proc. Natl. Acad. Sci. USA*, 2006, 103, 15729-15735.
3 D. G. Nocera, *Acc. Chem. Res.*, 2012, 45, 767-776.
4 M. Marszewski, S. Cao, J. Yu and M. Jaroniec, *Mater. Horiz.*, 2015, 2, 261-278.
5 A. Dhakshinamoorthy, S. Navalon, A. Corma and H. Garcia, *Energy Environ. Sci.*, 2012, 5, 9217-9233.
6 S. N. Habisreutinger, L. Schmidt-Mende and J. K. Stolarczyk, *Angew. Chem. Int. Ed.*, 2013, 52, 7372-7408.
7 A. Corma and H. Garcia, *J. Catal.*, 2013, 308, 168-175.
8 F. Sastre, A. V. Puga, L. Liu, A. Corma and H. Garcia, *J. Am. Chem. Soc.*, 2014, 136, 6798-6801.
9 A. V. Puga, *Top. Catal.* 2016, 59, 1268-1278.
10 X. Meng, T. Wang, L. Liu, S. Ouyang, P. Li, H. Hu, T. Kako, H. Iwai, A. Tanaka and J. Ye, *Angew. Chem. Int. Ed.*, 2014, 53, 11478-11482.
11 W. Sun, C. Qian, L. He, K. K. Ghuman, A. P. Wong, J. Jia, A. A. Jelle, P. G. O'Brien, L. M. Reyes, T. E. Wood, A. S. Helmy, C. A. Mims, C. V. Singh and G. A. Ozin, *Nat. Commun.*, 2016, 7, 12553.
12 H. Zhang, T. Wang, J. Wang, H. Liu, T. D. Dao, M. Li, G. Liu, X. Meng, K. Chang, L. Shi, T. Nagao and J. Ye, *Adv. Mater.*, 2016, 28, 3703-3710.
13 G. Chen, R. Gao, Y. Zhao, Z. Li, G. I. N. Waterhouse, R. Shi, J. Zhao, M. Zhang, L. Shang, G. Sheng, X. Zhang, X. Wen, L. Z. Wu, C. H. Tung and T. Zhang, *Adv. Mater.*, 2017, DOI: 10.1002/adma.201704663.
14 P. Lanzafame, S. Abate, C. Ampelli, C. Genovese, R. Passalacqua, G. Centi and S. Perathoner, *ChemSusChem*, 2017, 10, 4409-4419.
15 A. Navarrete, G. Centi, A. Bogaerts, Á. Martín, A. York and G. D. Stefanidis, *Energy Technol.*, 2017, 5, 796-811.
16 R. W. Dorner, D. R. Hardy, F. W. Williams and H. D. Willauer, *Energy Environ. Sci.*, 2010, 3, 884.
17 M. D. Porosoff, B. Yan and J. G. Chen, *Energy Environ. Sci.*, 2016, 9, 62-73.
18 G. Centi, E. A. Quadrelli and S. Perathoner, *Energy Environ. Sci.*, 2013, 6, 1711-1731.
19 A. Y. Khodakov, W. Chu and P. Fongarland, *Chem. Rev.*, 2007, 107, 1692-1744.
20 W. Wang, S. Wang, X. Ma and J. Gong, *Chem. Soc. Rev.*, 2011, 40, 3703-3727.
21 V. Iablokov, S. K. Beaumont, S. Alayoglu, V. V. Pushkarev, C. Specht, J. Gao, A. P. Alivisatos, N. Kruse and G. A. Somorjai, *Nano Lett.*, 2012, 12, 3091-3096.
22 M. P. Andersson, F. Abild-Pedersen, I. N. Remediakis, T. Bligaard, G. Jones, J. Engbæk, O. Lytken, S. Horch, J. H. Nielsen and J. Sehested, *J. Catal.*, 2008, 255, 6-19.
23 J. Gao, Q. Liu, F. Gu, B. Liu, Z. Zhong and F. Su, *RSC Adv.*, 2015, 5, 22759-22776.
24 A. Y. Khodakov, W. Chu and P. Fongarland, *Chem. Rev.*, 2007, 107, 1692-1744.
25 T. Riedel, M. Claeys, H. Schulz, G. Schaub, S.-S. Nam, K.-W. Jun, M.-J. Choi, G. Kishan and K.-W. Lee, *Appl. Catal. A: Gen.*, 1999, 186, 201-213.
26 Y. Zhao, B. Zhao, J. Liu, G. Chen, R. Gao, S. Yao, M. Li, Q. Zhang, L. Gu, J. Xie, X. Wen, L. Z. Wu, C. H. Tung, D. Ma and T. Zhang, *Angew. Chem. Int. Ed.*, 2016, 55, 4215-4219.
27 L. Liu, P. Concepción and A. Corma, *J. Catal.*, 2016, 340, 1-9.

28 L. Liu, F. Gao, P. Concepción and A. Corma, *J. Catal.*, 2017, 350, 218-225.
29 Riedel, T.; Claeys, M.; Schulz, H.; Schaub, G.; Nam, S.-S.; Jun, K.-W.; Choi, M.-J.; Kishan, G.; Lee, K.-W. *Appl. Catal. A: Gen.* **1999**, *186*, 201-213.
30 M. Ojeda, R. Nabar, A. U. Nilekar, A. Ishikawa, M. Mavrikakis and E. Iglesia, *J. Catal.*, 2010, 272, 287-297.
31 C. G. Visconti, M. Martinelli, L. Falbo, L. Fratalocchi and L. Lietti, *Catal. Today, 2016,* 277, 161-170.
32 J. Jia, H. Wang, Z. Lu, P. G. O'Brien, M. Ghoussoub, P. Duchesne, Z. Zheng, P. Li, Q. Qiao, L. Wang, A. Gu, A. A. Jelle, Y. Dong, Q. Wang, K. K. Ghuman, T. Wood, C. Qian, Y. Shao, C. Qiu, M. Ye, Y. Zhu, Z. H. Lu, P. Zhang, A. S. Helmy, C. V. Singh, N. P. Kherani, D. D. Perovic and G. A. Ozin, *Adv. Sci.*, 2017, 4, 1700252.
33 G. Simon, L. Meziane, A. Courty, P. Colomban, I. Lisiecki, *J. Raman Spectrosc.* 2016, 47, 248-251.
34 X. Deng, A. Verdaguer, T. Herranz, C. Weis, H. Bluhm and M. Salmeron, *Langmuir*, 2008, 24, 9474-9478.
35 M. Roiaz, E. Monachino, C. Dri, M. Greiner, A. Knop-Gericke, R. Schlogl, G. Comelli and E. Vesselli, *J. Am. Chem. Soc.*, 2016, 138, 4146-4154.
36 M.K. Gnanamani, G. Jacobs, R.A. Keogh, W.D. Shafer, D.E. Sparks, S.D. Hopps, G.A. Thomas, B.H. Davis, *Appl. Catal. A: General.*, 2015, 499, 39-46.
37 Y. Dai, F. Yu, Z. Li, Y. An, T. Lin, Y. Yang, L. Zhong, H. Wang, Y. Sun, *Chin. J. Chem.*, 2017, 35, 918-926.
38 P. Zhai, C. Xu, R. Gao, X. Liu, M. Li, W. Li, X. Fu, C. Jia, J. Xie, M. Zhao, X. Wang, Y. W. Li, Q. Zhang, X. D. Wen and D. Ma, *Angew. Chem. Int. Ed.*, 2016, 55, 9902-9907.
39 I. C. Yates, C. N. Satterfield, *Energy Fuels* 1991, 5, 168-173.
40 G. D. Weatherbee, C. H. Bartholomew, *J. Catal.* 1982, 77, 460-472.
41 S. Neatu, J. A. Macia-Agullo, P. Concepcion and H. Garcia, *J. Am. Chem. Soc.*, 2014, 136, 15969-15976.
42 C. H. Wu, B. Eren, H. Bluhm and M. B. Salmeron, *ACS Catal.*, 2017, 7, 1150-1157.
43 T. Ishida, T. Yanagihara, X. Liu, H. Ohashi, A. Hamasaki, T. Honma, H. Oji, T. Yokoyama and M. Tokunaga, *Appl. Catal. A: Gen.*, 2013, 458, 145-154.
44 M. Khobragade, S. Majhi and K. K. Pant, *Appl. Energy*, 2012, 94, 385-394.
45 M. Blanchard, H. Derule, P. Canesson, *Catal. Lett.*, 2, 1989, 319-322.
46 K. H. Cats and B. M. Weckhuysen, *ChemCatChem*, 2016, 8, 1531-1542.
47 A. C. Ferrari and J. Robertson, *Phys. Rev. B*, 2001, 64, 075414.
48 J. Yang, V. Frøseth, D. Chen and A. Holmen, *Surface Science*, 2016, 648, 67-73.
49 A. Y. Khodakov, *Catalysis Today*, 2009, 144, 251-257.
50 V. Navarro, M. A. van Spronsen and J. W. Frenken, *Nat. Chem.*, 2016, 8, 929-934.
51 S. W. T. Price, D. J. Martin, A. D. Parsons, W. A. Sławiński, A. Vamvakeros, S. J. Keylock, A. M. Beale, J. F. W. Mosselmans, *Sci. Adv.*, 2017, 3, e1602838.